In situ sequential STM imaging of structural changes resulting from the electrodissolution of silver crystal surfaces in aqueous perchloric acid: The roughening kinetics

M. E. Vela, G. Andreasen, R. C. Salvarezza, A. Hernández-Creus,* and A. J. Arvia
Instituto de Investigaciones Fisicoquímicas Teóricas y Aplicadas (INIFTA), Sucursal 4, Casilla de Correo 16, 1900 La Plata, Argentina
(Received 6 July 1995; revised manuscript received 7 December 1995)

Structural changes of silver terrace domains in aqueous perchloric acid solution at constant anodic current density (j) and room temperature were followed by *in situ* scanning tunneling microscopy sequential imaging. For $j<15$ μA cm^{-2} silver electrodissolution proceeds at step edges without roughening. Conversely, for $j>15$ μA cm^{-2} the silver surface becomes progressively rougher to attain, after a certain critical time, a steady roughness. In this case, the dynamic scaling theory applied to STM images indicates that the dissolving silver surface can be described as a self-affine fractal surface with a static roughening exponent $\alpha=0.90\pm0.06$, and a dynamic roughening exponent $\beta=0.36\pm0.08$. The value of α is consistent with the relevant role played by surface diffusion in the silver electrodissolution mechanism, whereas the value of β is slightly higher than those derived from growth models incorporating surface diffusion. The difference in the value of β would reflect the influence of either the electric field or energetic barriers at step edges on the rate of roughness development.

I. INTRODUCTION

Solid attack in aggressive environments involves a number of processes generally leading to the loss of material and development of an irregular surface topography. Although most of the research published on this matter emphasizes the former aspect in terms of either mass or current density, the development of a certain topography at the corroding surface becomes particularly relevant as it is closely related to the dissolution mechanism of the solid in the environment. In fact, the development of a particular topography at the nanometer level results from a competition among different physical processes operating at the reacting interface. Accordingly, the topography characterization on different scales together with those quantitative approaches to describe the development of irregular surfaces under nonsteady and stationary regimes appear to be most suitable to understand the mechanism of different corrosion processes from a nonconventional view.[1]

The electrodissolution of a pure metal in an aggressive environment at a low rate, occurring either spontaneously or assisted by an applied electric potential, implies the preferential removal of atoms at kink sites without an appreciable increase in the irregularity of the solid surface; i.e., the real surface area remains about the same. Conversely, the electrodissolution at a high rate involves the removal of surface atoms and void formation leading to the development of irregular topographies that in many cases can be described as fractals.[1] In both instances, the reaction front at the solid, often a strongly irregular front, shifts continuously inwards, and the overall process comprises the simultaneous atom detachment and vacancy formation at the solid surface, followed by the transport of dissolved species into the environment. The global reaction can be described by a complex reaction pathway in which the relaxation of surface atoms, either via surface tension[2] or surface diffusion[3] within the domain of the generated vacancy, plays a key role in surface smoothening. Therefore, surface particle relaxation implies that the minimum surface free energy compatible with either a stable or a metastable condition for the system is approached by changing the surface ordering.

In contrast to vapor deposition,[4] molecular beam epitaxy,[5] and metal electrodeposition,[6] few growth models have been discussed to describe the evolution of the topography of a solid under dissolution. Among them a model that involves the kinetic control of the process by the diffusion of ions outwardly has been proposed.[7] This model yields a topography of the reacting surface that is similar to the open self-similar fractal patterns resulting from diffusion-limited aggregation (DLA).[8] Likewise, a two-dimensional (2D) percolation model[9] has been advanced to explain the dissolution of metal alloys at potentials more negative than the critical potential for dealloying.[2]

When the dissolution of the solid can be described as a vacancy aggregation under surface reaction control, the entire corroding object would exhibit a rough self-affine fractal surface and a nonfractal mass. The analysis of this type of surface can be made, in principle, using the dynamic scaling theory,[5] which provides information about the kinetics and mechanism of roughening at the solid surface. However, neither experimental nor theoretical data have been found in the literature concerning the application of dynamic scaling to dissolving surfaces, in contrast to the formation of a new solid phase by electrodeposition.[10,11] It should be noted that, in general, there is evidence of roughening during the electrodissolution of metals and alloys in aggressive environments.[12]

This work reports the roughness evolution during the electrodissolution of silver single-crystal surface domains in contact with aqueous $1M$ $HClO_4$ derived from *in situ* sequential STM imaging. Silver electrodissolution in aqueous acid solution has been considered as an adequate model system for this purpose due to the high exchange current density of the $Ag^+(aq)/Ag(s)$ electrode reaction.[13,14]

Results reported here show that for low rates ($j<15$

 © 1996 The American Physical Society

μA cm^{-2}), silver electrodissolution proceeds without significant surface roughening, as has been recently reported for copper electrodissolution in chloride-containing solutions.[15] However, for higher electrodissolution rates ($j>15$ μA cm^{-2}) both void formation and smoothening can be observed. The silver surface, in this case, behaves as a self-affine fractal surface. The dynamic scaling analysis of scanning tunneling microscopy images resulting from $j>15$ μA cm^{-2} leads to a dynamic growth exponent, $\beta=0.36$, and the static growth exponent, $\alpha=0.9$. This value of α indicates that the fractal silver topography results from an electrochemical surface reaction in which silver surface atom diffusion plays a key role, whereas the value of β, which slightly exceeds the predictions of growth models incorporating surface diffusion, suggests that there is a contribution of either the electric field or energetic barriers at the step edges during the electrodissolution process leading to roughness.

II. EXPERIMENT

Electrochemical runs were performed in a Nanoscope III STM (Digital Instruments, Santa Barbara, CA) electrochemical equipment. The electrochemical cell consisted of a small Kel-F cell (1.1×2.0 cm^2 in size) in which an annealed polycrystalline silver (99.99%) plate working electrode (exposed area 0.5 cm^2), a large Pt counterelectrode, and a Pt reference electrode were lodged. The working electrode was mechanically polished first and then annealed at 400 °C under hydrogen. This procedure resulted in a Ag surface consisting of smooth terraces and steps a few atoms in height [Figs. 1(a)–1(c)]. In these STM images the 60° angle can be systematically observed at the intersection of steps, as expected for a Ag(111) surface. For silver, as in the case of gold, annealing results in a surface consisting of Ag(111) crystals. The presence of μm size ordered domains [Fig. 1(a)] made it possible to select smooth single-crystal surface domains 100 nm^2 in size to be followed by sequential STM imaging, when they were subjected to an applied potential to promote electrochemical metal dissolution.

Runs were made at $T=298$ K in an aqueous 1M (molar) $HClO_4$ working solution prepared from 70% analytical reagent $HClO_4$ and Milli-Q* water. The working solution was deaerated with purified nitrogen. Working electrode potential values given in the text were referred to the standard hydrogen electrode scale.

Silver electrodissolution runs were performed in the following way. First, the working electrode was polarized at $E=0.40$ V, i.e., a potential at which no silver electrodissolution occurred. Then, a smooth surface domain, typically 100 ×100 nm^2 in size, was chosen, and after drift attenuation, a series of STM images of this domain were taken for 15 min at null net faradaic current to assure that no change took place in the root-mean-square roughness at the working electrode surface. Afterwards, the constant current silver electrodissolution at an apparent current density in the range 4 μA cm$^{-2}<j<30$ μA cm^{-2} proceeded simultaneously with the sequential *in situ* STM imaging.

STM imaging was made using Pt-Ir nanotips covered by Apiezon wax to minimize the possible interference of faradaic currents. The following conditions for *in situ* STM imaging were used: tip potential (E_t), 0.50 $<E_t<$0.70 V, tunneling current $I_t=10$ nA, bias voltage $E_b=-0.2$ V, and frequency $f=5$ Hz. The value of E_{tip} was in the double-layer region of the tip material in the working solution and sufficiently positive to assure that silver dissolving from the substrate did not deposit on the tip. STM data were analyzed after fitting the instrument plane and applying a substracting procedure as described elsewhere.[22,23]

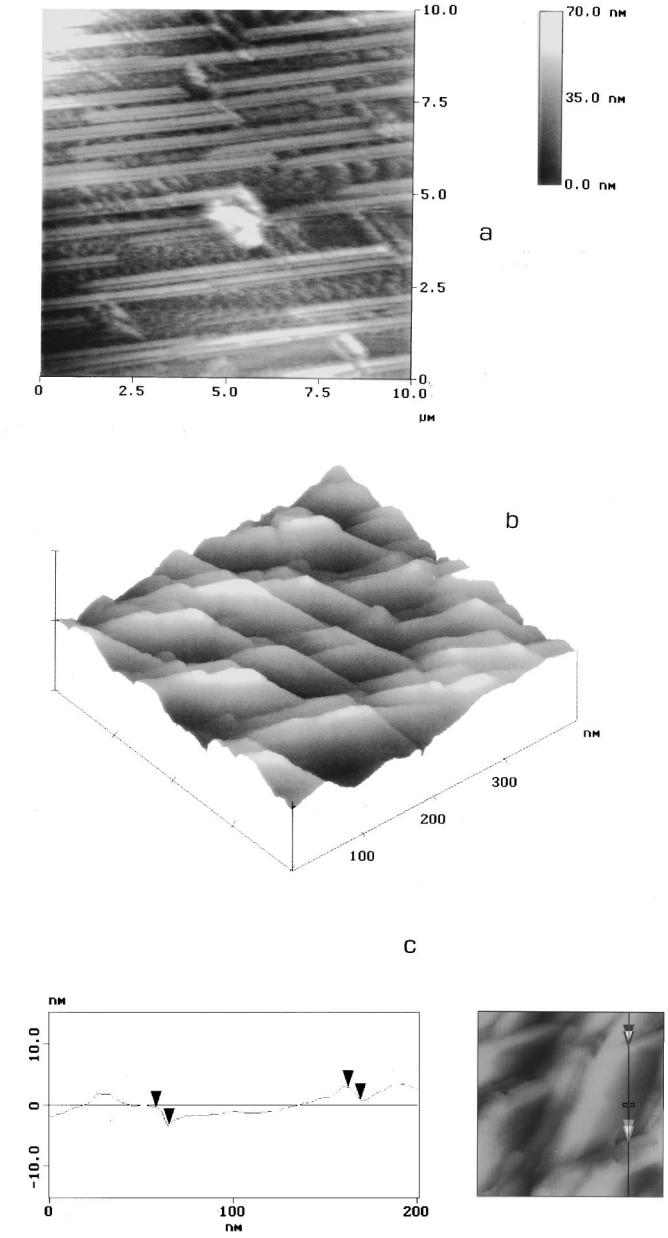

FIG. 1. (a) 10×10 μm^2 (top view) and (b) 400×400 nm^2 (3D view) *ex situ* STM images of the initial silver substrate. (c) Cross section of the initial silver substrate. Arrows indicate steps 8 atoms in height.

III. RESULTS AND INTERPRETATION

A. Electrochemical data

The voltammogram for the Ag electrode in 1M $HClO_4$ run at $v=0.02$ V s^{-1} between 0.25 and 0.9 V [Fig. 2(a)] in the positive-going potential scan shows a null current from

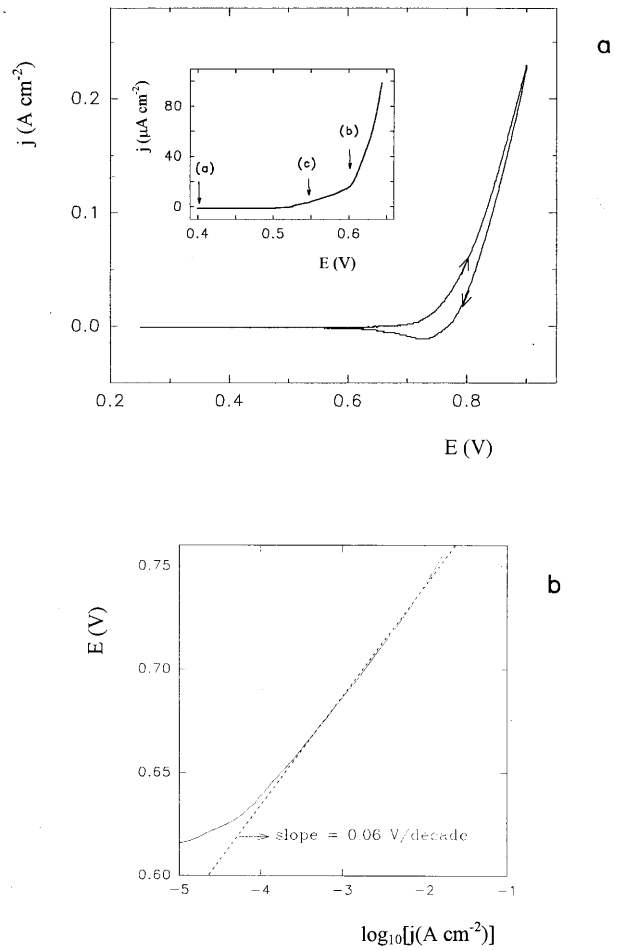

FIG. 2. (a) Voltammogram of a silver electrode in $1M$ $HClO_4$ recorded at 0.02 V s^{-1} between 0.25 and 0.9 V. $T=298$ K. The inset shows a detail of the initial anodic portion of the voltammogram. (b) A typical E vs $\log_{10} j$ curve obtained at 0.5 mV/s with a silver electrode in $1M$ $HClO_4$. $T=298$ K.

0.25 to 0.5 V, i.e., in the Ag(s)/$1M$ $HClO_4$(aq) double-layer region [see inset of Fig. 2(a)]. Silver electrodissolution commences at $E>0.5$ V. In the range 0.5–0.6 V the value of j, the apparent anodic current density, increases slightly with E, the applied potential, whereas for $E>0.6$ V, a remarkable increase in j is observed. Otherwise, the reverse potential scan exhibits a cathodic peak at $E=0.72$ V that is related to the electroreduction of Ag^+ ions formed in the preceding potential scan. According to the literature,[11,12] silver electrodissolution in the range $0.5<E<0.6$ is controlled by surface diffusion of Ag atoms, whereas for $E>0.6$ V, the $\ln j$ versus E plot [Fig. 1(b)] results in a straight line with the slope $b_a \cong 0.060$ V decade^{-1}, which is consistent with an electrochemical reaction controlled by the Ag^+ ion transport from the electrode to the solution.[13]

It is known that moving interfaces under mass transport control develop instabilities similar to those observed in the DLA model.[8] In this case, overhangs are produced during the interface motion that are inaccessible to STM measurements. Thus, the study of the evolution of Ag corroding interfaces has to be restricted to the range 0.5–0.6 V. The arrows denoted by a, b and c in the inset shown in Fig. 2(a) indicate the values of j chosen for *in situ* STM imaging.

B. Summary of the dynamic scaling theory

The concept of scaling was introduced in the field to provide a framework for understanding fractal-like topologies of nonequilibrium surfaces.[5] The dynamic scaling theory describes the development of a contour on a flat substrate consisting of N points and length L on the x axis at time $t=0$, and the surface roughness growth in a single direction normal to L (z axis) increasing in height h without overhangings. The instantaneous surface height can be described by the function $h(x,t)$. Then, $\xi(L,t)$, the instantaneous surface width, can be taken as a measure of the surface roughness. The value of $\xi(L,t)$ is given by the root-mean-square roughness of the interface height fluctuations.

For an irregular interface the dynamic scaling theory predicts that ξ scales with t and L as[5]

$$\xi(L,t) \propto L^{\alpha} f(x), \tag{1}$$

where $\xi(L,t)$ is defined by

$$\xi(L,t) = \left(1/N \sum \left[h(x_1) - \langle h \rangle \right]^2 \right)^{1/2}. \tag{2}$$

$h(x_1)$ is the deposit height measured along the x direction at the point x_i, and $x = t/L^{\alpha/\beta}$. Furthermore, $f(x)$ has the following properties: $f(x)=$const for $x \Rightarrow \infty$, and $f(x)=x^{\beta}$ for $x \Rightarrow 0$, β and α being the dynamic and static growth exponents, respectively. Note that according to the properties of $f(x)$ for $t \Rightarrow 0$ Eq. (1) is reduced to

$$\xi \propto t^{\beta}. \tag{3}$$

The value of the exponent β indicates the time evolution of the interface width of the growing surface. On the other hand, for $t \Rightarrow \infty$ Eq. (1) is reduced to

$$\xi \propto L^{\alpha}. \tag{4}$$

The value of α is related to the surface texture, and hence to D, the fractal surface dimension of the self-affine surface, by $D=3-\alpha$.[5] Thus, for $\alpha \Rightarrow 1$ ($D \Rightarrow 2$) the surface tends to be Euclidean (ordered), whereas when $\alpha \Rightarrow 0$ ($D \Rightarrow 3$) the surface exhibits an increasing degree of disorder. Key parameters α and β can be derived from the analysis of surface profiles resulting from adequate imaging procedures. In fact, this is the case of those profiles derived from images obtained by STM, which provide high lateral resolution 3D images in real space. Therefore, Eqs. (1)–(4) can be extended to data from STM images by replacing ξ by ξ_{STM}, the root-mean-square roughness resulting from STM profiles, and L by L_s, a segment of the STM scan. The values of the α and β exponents can be compared to those derived from atomistic and continuum models for interface evolution.[5]

Nonequilibrium growth conditions can be produced mainly under the influence of stochastic noise, site-dependent growth, and surface relaxation. Growth models based on an atomistic description such as the Eden,[16] ballistic deposition,[4] and restricted solid-on-solid[17] result in objects with a nonfractal mass and a self-affine fractal surface. The above-mentioned models can be successfully described by the Kardar, Parisi, and Zhang continuous equation[18] for interface motion, which leads to $\beta=0.25$ and $\alpha=0.4$ in 3D growth, and $\alpha+(\alpha/\beta)=2$ in all dimensions. Otherwise, those

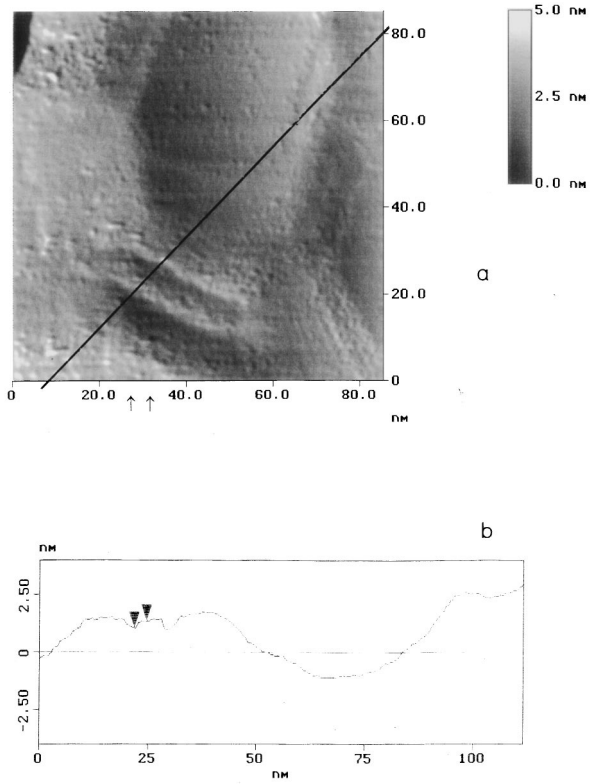

FIG. 3. (a) *In situ* STM image (top view) (85×85 nm^2, z=8 nm). (b) Cross-section analysis of a domain of the silver crystal shown in (a) in the direction of the solid line drawn in (a). Arrows indicate a step 1 atom in height. Image taken at a constant applied potential E_c=0.40 V in $HClO_4$ 1M. T=298 K.

models incorporating surface diffusion lead to either α=1.0 and β=0.25,[19,20] or α=0.66 and β=0.20,[21] fulfilling the predictions of the linear surface diffusion equation, α/β=4.

C. *In situ* STM imaging

The *in situ* STM image 85×85 nm^2 in size [Fig. 3(a)] corresponding to a single-crystal domain taken at null current [arrow *a* in Fig. 2(a), E=0.40 V], i.e., in the absence of a net Ag electrodissolution, shows a smooth surface surrounded by steps of a single atom in height [Fig. 3(b)]. The central part of the single-crystal domain is depressed with respect to the crystal edges [Fig. 3(b)], in agreement with results already reported in the literature.[24]

When a net anodic current flows through the electrode [j=30 μA cm^{-2}, arrow *b* in Fig. 2(a)], a drastic change takes place in the silver electrode topography (Fig. 4). Sequential STM images 85×85 nm^2 in size [Figs. 4(a)–4(d)] show the progressive development of a rough surface caused by the

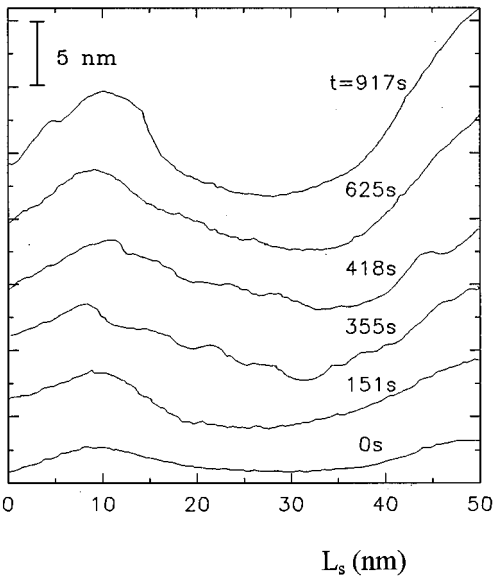

FIG. 5. Typical STM cross sections of surfaces depicted in Fig. 4. The electrodissolution time is indicated for each curve. L is the length of the image measured in the fast STM scan axis.

silver crystal electrodissolution. This can be clearly seen, for instance, in Fig. 5 where typical STM cross sections of the silver surface are depicted. They demonstrate that the initially smooth profile develops large instabilities growing in time. Furthermore, small voids are also formed during silver electrodissolution although they rapidly disappear by smoothing.

The change in the silver topography resulting from the electrodissolution at j=30 μA cm^{-2} can be expressed through the change in ξ_{STM}, the root-mean-square roughness resulting from STM images. Thus, the ξ_{STM} versus t (Fig. 6) plot exhibits an initial increase in ξ_{STM} with t, and afterwards, for $t>\tau$=600 s a constant ξ_{STM} value is attained, indicating that a steady-state roughening regime has been reached [Fig. 6(a)]. It is worth noting that the overall anodic charge involved in this experiment is equivalent to the removal of 150 silver monolayers or thereabout. From the initial portion of the ξ_{STM} versus t plot (Fig. 6), the value of β can be obtained since

$$\xi_{STM} \propto t^{\beta}. \tag{5}$$

Hence, by plotting $\log_{10} \xi_{STM}$ versus $\log_{10} t$ for $t<\tau$ it results in β=0.36±0.08 (Fig. 7).

Reliable values of α can also be obtained from STM images by using the single-image dynamic scaling method[25]

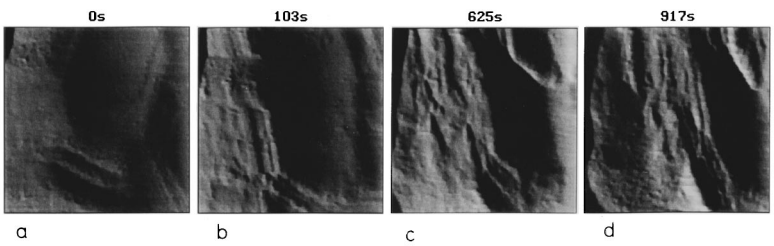

FIG. 4. Sequential STM images (top view) (85×85 nm^2) obtained during the electrodissolution of silver in 1M $HClO_4$ at j=30 μA cm^{-2} [(b)–(d)]. The electrodissolution time is indicated in the upper part of each picture. (a) corresponds to the initial silver surface at E=0.40 V under the null current condition. T=298 K.

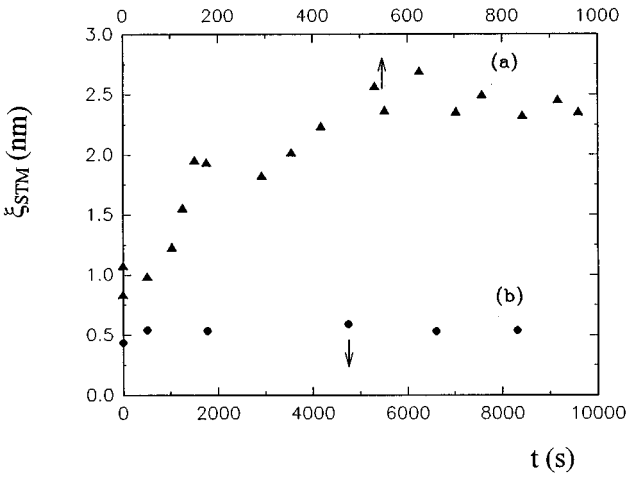

FIG. 6. (a) (▲) ξ_{STM} vs t plot at $j=30$ μA cm^{-2}. (b) (●) ξ_{STM} vs t plot at $j=4$ μA cm^{-2}.

taking data in the steady-state roughness regime, i.e., $t>\tau$. Then, the value of α can be obtained from the equation

$$\xi_{STM} \propto L_s^{\alpha}, \tag{6}$$

where L_s is the length of a segment of the STM scan of size S measured in the fast scanning direction (x) by plotting $\log_{10}\xi_{STM}$ versus $\log_{10} L_s$ from STM images (Fig. 8). These plots exhibit a straight line portion with the slope $\alpha=0.86 \pm 0.01$ for $\log_{10} L_s<1.5$, and a saturation region for $\log_{10} L_s>1.5$.

It should be noted that for computer simulated fractals, data covering 4–5 orders of magnitude are required for logarithmic fitting. For experimental systems, however, the goal is less ambitious owing to the existence of inner and outer cutoffs. Then, $\log_{10}\xi_{STM}$ versus $\log_{10} L_s$ linear plots covering at least one order of magnitude or thereabout can be considered acceptable.[26]

The sequential *in situ* STM imaging of the dissolving silver surfaces was also obtained by setting $j=4$ μA cm^{-2} [arrow c in Fig. 2(a)] for $t=10^4$ s, i.e., a charge density equivalent to the removal of 150 silver monolayers or thereabout. In this case, STM images change with time although the value of ξ_{STM} remains constant. This means that the electrodissolution proceeds from the steps without roughening of the silver surface for at least 10^4 s [Fig. 6(b)]. This implies $\beta=0$; i.e., a layer-by-layer dissolution process seems to operate at the silver surface. This mode of electrodissolution has been recently reported for copper in chloride-containing solutions.[15]

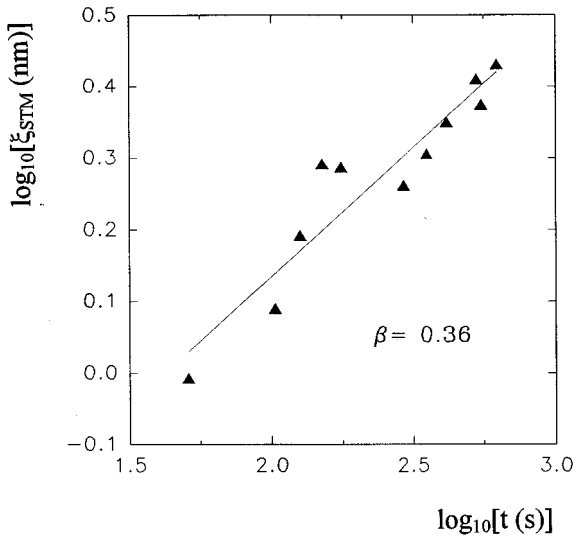

FIG. 7. $\log_{10}\xi_{STM}$ vs $\log_{10} t$ plot for the electrodissolution of silver at $t<600$ s.

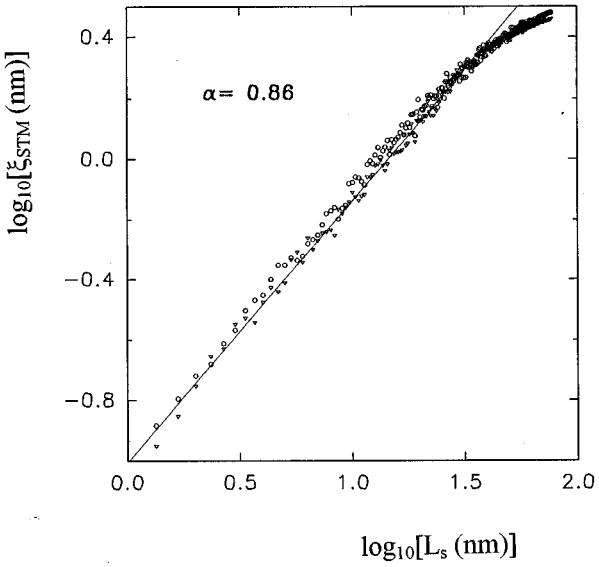

FIG. 8. $\log_{10}\xi_{STM}$ vs $\log_{10} L_s$ plot for the electrodissolution of silver in the saturation roughness regime.

Finally, in some runs made at a net null current the evolution of steps emerging at screw dislocations at silver terraces was followed by *in situ* sequential STM images [Figs. 9(a)–9(c)]. Unstable monoatomic steps displace over the surface to reach stable step edges. Then, from the value of d, the distance between the stable step and the unstable step edge, measured at different time t, and the relationship $d^2=\pi Dt$, the value of D, the rate constant for the step movement, was evaluated. It resulted in $D=10^{-13}$ cm^2 s^{-1}. It should be noted that STM images of step edges at higher magnifications show frizzy steps 1 nm in average width. This figure agrees with the average width of frizzy steps, which has been observed for Ag(111) in aqueous sulfuric acid at similar overpotential and temperature.[27] The appearance of frizzy steps confirms the high surface mobility of silver at the electrochemical interface.

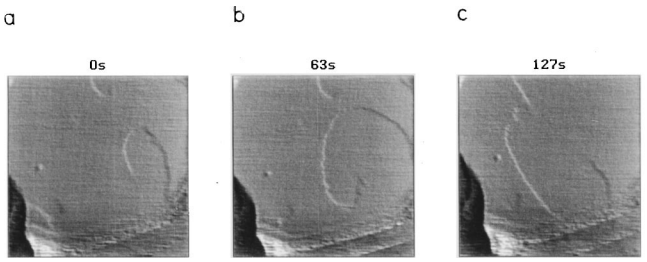

FIG. 9. (a)–(c) Sequential STM images (top view) (115×115 nm^2) of silver in 1M $HClO_4$ obtained at null current and $E=0.4$ V. The electrodissolution time is indicated in the upper part of each picture.

IV. DISCUSSION

A. Surface diffusion and roughening

The preceding analysis and interpretation of results have pointed out two important features related to a silver surface in contact with the working acid solution, namely, the high surface mobility of the silver surface even at null net faradaic current, and the change in the dissolution mode according to the magnitude of the faradaic current. The former aspect confirms recently reported findings concerning the appearance of frizzy steps at STM images of a silver single crystal in contact with aqueous acid solutions,[27] and roughness relaxation of fresh silver deposits produced by the electrodissolution of silver in chloride-containing solutions,[28] a matter that is of particular interest in the theoretical interpretation of the surface enhancement Raman spectroscopy.[29]

The layer-by-layer dissolution mode of silver surfaces observed by STM at low current densities is consistent with atom removal at step edges with high kink density. Then, the electrodissolution of silver implies the ionization of Ag atoms at kink sites followed by the transport of Ag^+ ions to the solution. The overall process may involve silver atom surface diffusion before the ionization step takes place.[13,30] Electrochemical kinetic data on silver electrodeposition and electrodissolution in aqueous environments at room temperature and low overpotentials have revealed that the surface diffusion step is rate determining.[13,30] Accordingly, the layer-by-layer silver dissolution occurs without roughening of the reacting interface; i.e., in this case, the silver surface can be described as a Euclidean object.

From the standpoint of roughness development, the dynamic scaling theory applied to STM data indicates that the silver surface under anodic electrodissolution at $j>15$ μA cm^{-2} can be described as a self-affine fractal with $\alpha=0.9$ and $\beta=0.36$.

To account for both the results and interpretation advanced in this work, different models based on 3D Monte Carlo simulation for the dissolution of a solid were investigated to get a quantitative explanation of the roughness exponents, and to establish the influence of surface diffusion on the topography of the dissolving solid.

B. Monte Carlo modeling

Three-dimensional Monte Carlo simulations for the dissolution of a solid substrate were performed on the basis of the procedure already described for the two-dimensional case.[31] Simulations were made based on a substrate initially consisting of a cubic lattice either 60×60×60, 80×80×26, 90×90×20, or 100×100×17 in grid size. From the standpoint of particle dynamics, two principal models were considered.

In the first model (model I) the random particle detachment from the smooth substrate surface implies a site-dependent detachment probability, $P_d(N)$, given by

$$P_d(N)=6-N/3, \tag{7}$$

where N is the coordination number of the detaching particle at the substrate surface. This dissolution model generates "noisy" surfaces similar to those obtained in ballistic aggregation.[4] From the application of the dynamic scaling [Eqs. (3) and (4)] to the computer generated surfaces the following set of roughening exponents, $\alpha=0.4$ for $\langle h\rangle \gg L$ ($t\Rightarrow\infty$), and $\beta=0.23$ for $\langle h\rangle \ll L$ ($t\Rightarrow 0$) was obtained. These figures agree with the expectations of the Kardar, Parisi, and Zhang continuous equation for interface motion,[18] but they are far from experimental data on electrodissolution of silver surfaces at low and high current densities.

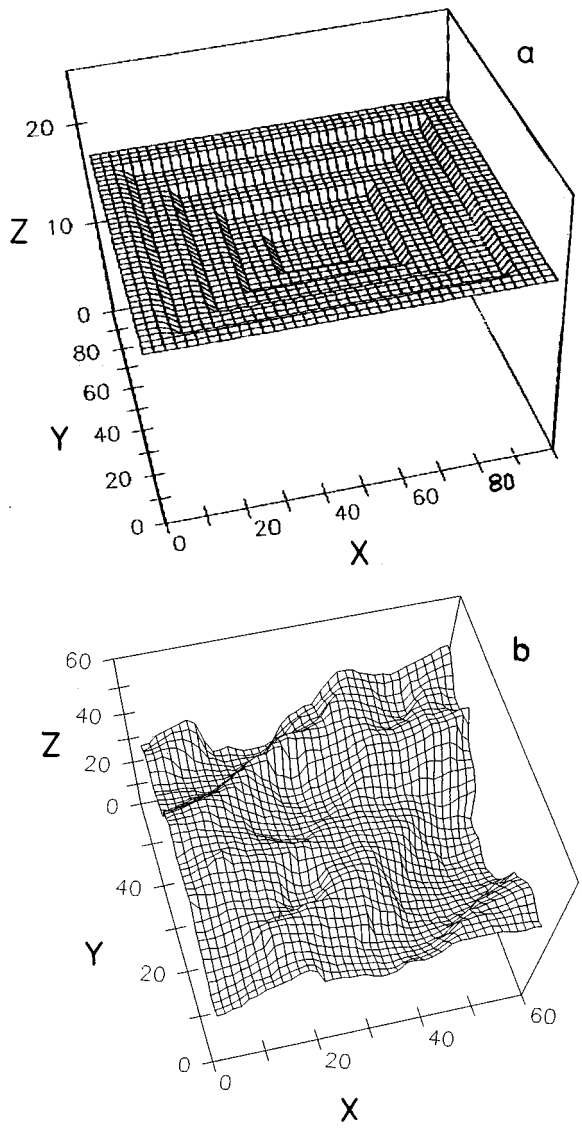

FIG. 10. (a) Initial 3D substrate model with a depressed center used in the Monte Carlo simulation of solid dissolution. (b) Snapshot of a 3D surface resulting from the Monte Carlo simulation of solid dissolution including adatom surface diffusion l_{dM} (model II).

In the second model (model II) particle detachment also occurs as in model I, but after the particle detachment neighboring particles around the created vacancy are allowed to diffuse on the substrate surface within a certain maximum length l_{dM} to reach a site with a higher N. Surface diffusion of particles takes place with the same probability in all directions. The 3D Monte Carlo simulation from model II leads to $\alpha=0.95$ for $\langle h\rangle \gg L$ ($t\Rightarrow\infty$), and $\beta=0.23$ for $\langle h\rangle \ll L$ ($t\Rightarrow 0$), irrespective of the value of l_{dM}. The same roughening exponents were obtained when the simulation implied a starting substrate surface depressed at the lattice center [Fig. 10(a)], a situation often observed in silver single-crystal surfaces.[24] Thus, the roughness exponents remain insensitive

to the change in the starting substrate topography. These values of α and β are within the range $\alpha=1$ and $\beta=0.25$ resulting from those aggregation models incorporating surface diffusion.[18,19] In fact, the values of α and β derived from model II are not far from $\alpha=0.9$ and $\beta=0.35$ resulting from the silver electrode topography under anodic electrodissolution at $j>15$ μA cm^{-2}. The 3D snapshots generated by model II show a smooth topography in which large instabilities are produced [Fig. 10(b)] resembling closely the experimental STM images. Therefore, Monte Carlo simulation favors a description of roughness development during silver electrodissolution in which surface atom diffusion plays a key role.

The main difference between the theoretical predictions of model (ii) and the experimental data lies in the value of β, as the experimental value $\beta=0.35$ is greater than $\beta=0.23$ resulting from the model. This discrepancy is similar to that observed for other experimental systems, and it is suspected to be caused by the contribution of ''nonlocal effects,''[10] i.e., when the properties of the reacting surface site do not depend entirely on processes at the surface itself but on a Laplacian field acting in the environment.[10] In the case of metal electrodeposits the contribution of the electric field operating at the metal-solution interface would induce instabilities leading to larger β values.[10,32] It should be noted that energetic barriers at step edges would also result in a change from $\beta=0.25$ to 0.5, as concluded from Monte Carlo simulations of growth processes where interlayer mass transport is inhibited.[33]

C. The surface diffusion coefficient of silver atoms

The contribution of surface diffusion to the topography of Ag surfaces in contact with aqueous electrolyte solutions can be evaluated from the results depicted in Figs. 9(a) and 9(b). From an atomistic point of view, the curved steps contain a high density of kinks. In this configuration, the energetic content of the step is very high because of the large number of broken bonds of atoms with a low coordination number. Then, moving Ag adatoms from small dissolving clusters are attached to curved steps to form facets in order to decrease the surface free energy. The overall mass transport process at the surface explains the smoothening of small voids during the electrodissolution at high current densities.

Assuming that the shift of step edge in Figs. 9(a)–9(c) is controlled by the arrival of silver atoms by surface diffusion at the terraces, the surface diffusion coefficient of Ag atoms at the Ag/1M $HClO_4$ aqueous interface should be of the order of 10^{-13} cm^2 s^{-1}. This figure is 1 order of magnitude greater than that expected for Ag atoms at a silver surface in vacuum at the same temperature.[34] This enhancement of Ag atom surface diffusion in going from vacuum to the aqueous solution environment is qualitatively and quantitatively similar to that recently reported for Au atom surface diffusion on a gold surface.[35] For both metals, this difference can be related to specific applied potential-dependent interactions involving solution constituents and the metal surface. Unlike strongly adsorbed immobile species,[36] the complex-metal-ion-forming anions increase the value of the surface diffusion coefficient of metal atoms.

V. CONCLUSIONS

On the basis of the analysis of *in situ* STM images we have demonstrated that the interface of an electrodissolving single-crystal metal surface at high current densities can be described as a self-affine fractal. The development of this rough topography under nonequilibrium conditions involves the noise introduced by the random nature of the dissolution process and silver atom surface diffusion, which reflect in the value of α. The value of β indicates that either the electric field or the presence of energetic barriers at step edges also participates in the kinetics of roughness development. At low current densities, the properties of the dissolving silver surface are compatible with the layer-by-layer dissolution model developed from thermodynamic equilibrium conditions.

Mechanistic conclusions derived from the dynamic scaling analysis agree with those previously derived from silver electrode kinetic data.

ACKNOWLEDGMENTS

This work was financially supported by the Consejo Nacional de Investigaciones Científicas y Técnicas of Argentina (CONICET).

*Visiting Professor from Departamento de Química-Física, Universidad de La Laguna, Tenerife, Spain.

[1] G. Daccord, in *The Fractal Approach to the Heterogeneous Chemistry*, edited by D. Avnir (Wiley, New York, 1989), p. 183.
[2] K. Sieradzki, J. Electrochem. Soc. **140**, 2868 (1983).
[3] J. R. Galvele, Corros. Sci. **27**, 1 (1987).
[4] P. Meakin, P. Ramanlal, L. M. Sander, and R. C. Ball, Phys. Rev. A **34**, 509 (1986).
[5] F. Family, Physica A **168**, 561 (1990), and references therein.
[6] P. Meakin, in *The Fractal Approach to the Heterogeneous Chemistry* (Ref. 1), p. 131.
[7] M. I. J. Beale, J. D. Benjamin, M. J. Uren, N. G. Chew, and A. G. Cullis, J. Cryst. Growth **75**, 408 (1986).
[8] T. A. Witten and L. M. Sander, Phys. Rev. Lett. **47**, 1400 (1981).
[9] P. Evesque, in *The Fractal Approach to the Heterogeneous Chemistry* (Ref. 1), p. 81.
[10] A. Iwamoto, T. Yoshinobu, and H. Iwasaki, Phys. Rev. Lett. **72**, 4025 (1994).
[11] P. Ocón, P. Herrasti, J. M. Vara, L. Vázquez, R. C. Salvarezza, and A. J. Arvia, J. Phys. Chem. **98**, 2418 (1994).
[12] D. W. Suggs and A. J. Bard, J. Am. Chem. Soc. **116**, 10 725 (1994).
[13] W. Mehl and J. O'M. Bockris, Can. J. Chem. **37**, 190 (1959).
[14] A. V. Vvedenskii and I. K. Marshakov, Russ. J. Electrochem. **31**, 234 (1995).
[15] D. W. Suggs and A. J. Bard, J. Phys. Chem. **99**, 8349 (1995).
[16] M. Eden, in *Proceedings of the 4th Berkeley Symposium on Mathematical Statics and Probability*, edited by F. Neyman (University of California Press, Berkeley, 1961), Vol. 4.
[17] G. H. Gilmer and P. Bennema, J. Appl. Phys. **43**, 1347 (1992).
[18] M. Kardar, G. Parisi, and Y. C. Zhang, Phys. Rev. Lett. **56**, 889 (1986).

[19] D. E. Wolf and J. Villain, Europhys. Lett. **13**, 389 (1990); J. Villain, J. Phys. (France) I **1**, 19 (1992).
[20] M. Siegert and M. Plischke, Phys. Rev. Lett. **73**, 1517 (1994).
[21] Z. W. Lai and S. Das Sarma, Phys. Rev. Lett. **66**, 2348 (1991).
[22] L. Vázquez, R. C. Salvarezza, P. Herrasti, P. Ocón, J. M. Vara, and A. J. Arvia, Appl. Surf. Sci. **70–71**, 413 (1993).
[23] J. Krim, I. Heyvaert, C. Van Haesendonck, and Y. Bruynseraede, Phys. Rev. Lett. **70**, 57 (1993).
[24] L. Vázquez, A. Hernández-Creus, P. Carro, P. Ocón, P. Herrasti, C. Palacio, J. M. Vara, R. C. Salvarezza, and A. J. Arvia, J. Phys. Chem. **96**, 10 454 (1992).
[25] R. C. Salvarezza, L. Vázquez, P. Herrasti, P. Ocón, J. M. Vara, and A. J. Arvia, Europhys. Lett. **20**, 727 (1992).
[26] C. Thompson, G. Palasantzas, Y. P. Feng, S. K. Sinha, and J. Krim, Phys. Rev. B **49**, 4902 (1994); P. Pfeifer, Y. J. Wu, M. W. Cole, and J. Krim, Phys. Rev. Lett. **62**, 1997 (1989).
[27] M. Dietterle, T. Will, and D. Kolb, Surf. Sci. **327**, L495 (1995).
[28] J. S. Chen, T. M. Devine, D. F. Ogletree, and D. M. Salmeron, Surf. Sci. **258**, (1991).
[29] A. Otto, Phys. Rev. B **27**, 5132 (1983).
[30] H. Gerischer and R. P. Tischer, Z. Elektrochem. **61**, 1159 (1957).
[31] A. Hernández-Creus, P. Carro, R. C. Salvarezza, and A. J. Arvia, J. Electrochem. Soc. **142**, 3806 (1995).
[32] L. Vázquez, R. C. Salvarezza, P. Herrasti, P. Ocón, J. M. Vara, and A. J. Arvia, Phys. Rev. B **52**, 2032 (1995).
[33] Z. Zhang, J. Detch, and H. Matiu, Phys. Rev. B **48**, 4972 (1993).
[34] G. E. Rhead, Surf. Sci. **47**, 207 (1975), and references therein.
[35] M. P. García, M. M. Gómez, R. C. Salvarezza, and A. J. Arvia, J. Electroanal. Chem. **347**, 237 (1993).
[36] C. Alonso, R. C. Salvarezza, J. M. Vara, and A. J. Arvia, Electrochim. Acta **35**, 1331 (1990).

View publication stats